Oscillation and evolution characteristics of nanofluid thermocapillary convection in rectangular cavity

Xiaoming Zhou [a], Cheng Dai [a], Yanni Jiang [a,*], Qisheng Chen [b]

[a] College of Mechanical and Electrical Engineering, Hohai University, China
[b] Institute of Mechanics, Chinese Academy of Sciences, China

ARTICLE INFO

ABSTRACT

To analyze the oscillation and evolution characteristics of nanofluid thermocapillary convection instability, a two-phase mixture model was utilized to simulate nanofluid thermocapillary convection in a rectangular cavity and investigate the impact of nanoparticle volume fraction on the oscillatory flow. The results indicate that the two-phase mixture model has a lower critical temperature difference compared to the single-phase model, and the oscillation mode exhibits distinct changes for small nanoparticle volume fractions. At a high Marangoni number, the thermocapillary convection displays periodic oscillatory behavior, with the flow field composed of several dynamic convection vortices. An increase in nanoparticle volume fraction results in a decrease in the critical temperature difference, as well as the amplitude and variation range of temperature oscillation. However, the oscillation period shows an approximate linear increase. Furthermore, there is a non-uniform distribution of nanoparticles at the vicinity of solid wall, especially a significant concentration gradient near the side wall.

1. Introduction

Thermocapillary flow is the predominant form of spontaneous convection in the microgravity environment of space, where surface tension fluctuates with temperature and the inhomogeneity of surface tension becomes the driving force of liquid flow. After Smith and Davis first proposed the thermocapillary convection instability mode of the hydrothermal wave [1], other researchers thoroughly investigated the instability of thermocapillary convection with single-phase fluids [2–5]. The aspects studied are the role of the Prandtl number, aspect ratio, and Marangoni number on thermocapillary convection properties [6,7]. To explore new ways to change the low thermal conductivity and poor heat transfer performance of typical fluidic workpieces, Choi and Eastman first studied nanofluids in 1995 [8]. A nanofluid comprises a stable and homogeneous suspension formed by adding nanoscale particles of metal or non-metal oxide to a base fluid. Nanofluids, known for their exceptional efficiency and heat transfer performance, offer promising prospects in the realms of heat transfer enhancement and renewable energy utilization. Since their introduction, nanofluids have garnered significant attention from researchers [9–13]. In the study conducted by M. Sheikholeslami [14–21], Darcy law was utilized to simulate the flow of MHD in porous media, revealing a weakening of convection with the

increase in magnetic force and an influence of radiation on the distribution of temperature gradients. Moreover, porous media simulations utilize non-Darcy's law, and the investigation focuses on studying the transport characteristics and entropy generation of magnetic nanofluids. Nanofluid thermocapillary convection, an important subfield of nanofluids, finds applications in diverse areas, including microfluidic channels and heat pipes [22–24]. As a result, nanofluid thermocapillary convection has garnered considerable interest from scientists.

Aminfar et al. [25] accounts for gravity when examining thermocapillary convection features. The relationship between the volume fraction and the properties of nanofluid thermocapillary convection in the floating zone is demonstrated. The buoyant-Marangoni convection in a steady state was explored numerically by Saleh et al. [26]. This study investigated how the nanoparticle volume fraction affects the fluid structure and velocity, and how the different nanoparticles affect the critical Marangoni number. Kolsi [27] focused on the numerical study of buoyancy and thermocapillary convection in a three-dimensional rectangular liquid cavity, the simulations concentrated on the impact of Marangoni number and nanoparticle volume fraction on entropy. Heikholeslami et al. [28] studied the MHD influence on the steady-state Marangoni convection of nanofluids. Abdullah et al. [29] used a linear stability analysis method for thin liquid-layer nanofluid Marangoni convection at a vertical temperature difference and found that

* Corresponding author.
  E-mail address: ynjiang@hhu.edu.cn (Y. Jiang).

Nomenclature		ρ	density, kg/m^3
		μ	dynamic viscosity, Pa s
a	acceleration, m^2/s	λ	thermal conductivity, W/m K
C_p	specific heat, J/kg K	Y_T	surface tension temperature coefficient, N/m K
Pr	Prandtl number, $\text{Pr} = C_p\mu/\lambda$	α	volume fraction
T	temperature, K		
P	pressure, Pa	*Subscipts*	
t	time, s	f	the base fluid
$\overrightarrow{V}$	the velocity vector, m/s	nf	nanofluid
H	Height, m	p	nanoparticles
L	Length, m	h	hot
		c	cold
Greek symbols		k	the kth phase
τ	oscillatory period, s	n	the number of phases

nanoparticle volume fraction and size are intimately linked to flow patterns. Gevorgyan et al. [30] decided to irradiate the nanofluid using a laser in order to heat the nanofluid and monitor the change in flow velocity. It was also further analyzed by changing the light intensity and nanoparticle concentration. Jiang et al. [31] considered the influence of the complex relationship between nanoparticles and surface tension on thermocapillary convection, focusing on convective strength and entropy changes of nanofluids.

Currently, research is being conducted on nanofluid thermocapillary convection using primarily single-phase and mixed models. Zhou et al. [32] examined the oscillation properties and development of nanofluid thermocapillary convection at moderate Prandtl number, demonstrating the fluctuation of the critical Marangoni number and flow forms at different nanoparticle volume fractions. However, a single-phase model cannot disclose the precise distribution of nanoparticle concentration and cannot more accurately represent the properties of the nanofluid. As is common knowledge, because nanofluid is a mixed fluid, factors such as gravity, friction between nanoparticles and the base fluid, Brownian force, settling, and diffusion phenomena have an impact on the fluid flow, causing a slip velocity relative to the continuous phase. The findings will be more accurate if numerical simulations are performed using the mixture model. Jiang [33] investigated nanofluid's steady-state thermocapillary convection numerically using two-phase mixture model, revealing the impact that nanoparticles had on the thermocapillary convection and the free surface velocity. Chen [34] numerically simulated the steady-state thermocapillary convection of a graphene nanofluid while in microgravity using a two-phase mixture model, without investigating the nanofluid thermocapillary convection oscillatory features.

At present, the research on the flow instability of nanofluid thermocapillary convection relies mainly on single-phase model, which is straightforward theoretically and requires little computing effort. However, more precise findings will be obtained by using a two-phase mixture model. Therefore, the primary goals of this paper are to clarify the difference between the two-phase mixture model and the single-phase model, and more accurately reveal the oscillation characteristics and evolution process of nanofluid thermocapillary convection.

2. Physical and mathematical model

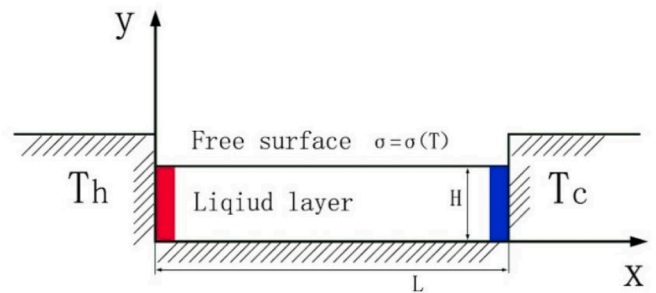This paper uses the rectangular liquid cavity model with horizontal

Fig. 1. Physical model.

temperature difference heating to research the thermocapillary convection instability. The rectangular liquid cavity shown in Fig. 1 has length L and height H (L = 20 mm and H = 3 mm). The left and right ends have a temperature difference of ΔT ($\Delta T = T_h\text{-}T_c$), with the left end being hot and the right end being cold. The liquid is considered to be in an ideal state, adiabatic with respect to the air and the bottom, and undeformed. The left and right walls are heated slightly to explore thermocapillary convection instability of nanofluids in laminar flow. Only the situation where surface tension has a linear relationship with temperature is studied in this work. Additionally, the buoyant convection is not accounted for. Inside the cavity, the initial velocity field is zero, and the starting temperature is T= $(T_h + T_c)/2$. The two-phase mixture model considers the velocity difference between the particle phase and the liquid phase, which makes the calculation results more accurate than the single-phase model and does not increase much computational resources. For the numerical analysis of nanofluid thermocapillary convection in this paper, the two-phase mixture model with the following control equation is employed [35].

Continuity equation:

$$\frac{\partial \rho_{nf}}{\partial t} + \nabla\hat{A}\cdot\left(\rho_{nf}\overrightarrow{V}_{nf}\right) = 0 \tag{1}$$

Momentum equation:

$$\frac{\partial\left(\rho_{nf}\overrightarrow{V}_{nf}\right)}{\partial t} + \nabla\hat{A}\cdot\left(\rho_{nf}\overrightarrow{V}_{nf}\overrightarrow{V}_{nf}\right) = -\nabla P + \nabla\hat{A}\cdot\left[\mu_{nf}\left(\nabla\overrightarrow{V}_{nf} + \left(\nabla\overrightarrow{V}_{nf}\right)^{\text{T}}\right)\right] + \nabla\hat{A}\cdot\left(\sum_{k=1}^{n}\alpha_k\rho_k\overrightarrow{V}_{dr,k}\overrightarrow{V}_{dr,k}\right) \tag{2}$$

Energy equation:

$$\frac{\partial}{\partial t}\left(\sum_{k=1}^{n}\alpha_k\rho_k E_k\right) + \nabla\hat{A}\cdot\sum_{k=1}^{n}\alpha_k\overrightarrow{V}_k(\rho_k E_k + P) = \nabla(\lambda_{nf}\nabla T) \tag{3}$$

$$E_k = h_k - \frac{P}{\rho_k} + \frac{\overrightarrow{V}_k^2}{2} \tag{4}$$

In the equation above, $\overrightarrow{V}_{nf}$ is the mass-averaged velocity, m/s, $\overrightarrow{V}_{dr,k}$ is the drift velocity of the kth phase. Formula 4 is applied to the compressible phase; the incompressible phase with $E_k = h_k$, where h_k is the sensible enthalpy of phase k.

$$\rho_{nf} = \sum_{k=1}^{n}\alpha_k\rho_k \tag{5}$$

$$\overrightarrow{V}_{nf} = \frac{\sum_{k=1}^{n}\alpha_k\rho_k\overrightarrow{V}_k}{\rho_{nf}} \tag{6}$$

$$\mu_{nf} = \sum_{k=1}^{n}\alpha_k\mu_k \tag{7}$$

$$\overrightarrow{V}_{dr,k} = \overrightarrow{V}_k - \overrightarrow{V}_{nf} \tag{8}$$

The slip velocity represents that of the second phase (nanoparticle, p) with respect to the first phase (base fluid, f):

$$\overrightarrow{V}_{pf} = \overrightarrow{V}_p - \overrightarrow{V}_f \tag{9}$$

The following equation represents the relationship between drift velocity and slip velocity:

$$\overrightarrow{V}_{dr,p} = \overrightarrow{V}_{pf} - \frac{\alpha_p\rho_p}{\rho_{nf}}\left(\overrightarrow{V}_f - \overrightarrow{V}_p\right) \tag{10}$$

Volume fraction equation of nanoparticles (p):

$$\frac{\partial(\alpha_p\rho_p)}{\partial t} + \nabla\hat{A}\cdot\left(\alpha_p\rho_p\overrightarrow{V}_{nf}\right) = -\nabla\hat{A}\cdot\left(\alpha_p\rho_p\overrightarrow{V}_{dr,p}\right) \tag{11}$$

Equation (12), published by Manninen et al. [36], calculates the slip velocity, and equation (13), proposed by Schiller and Naumann [37], calculates the drag function f_{drag}.

$$\overrightarrow{V}_{pf} = \frac{\rho_p d_p^2}{18\mu_{nf}f_{drag}}\frac{\rho_p - \rho_f}{\rho_p}\overrightarrow{V}_f\overrightarrow{a} \tag{12}$$

$$f_{drag}\begin{cases} 1 + 0.15Re_p^{0.687}Re_p \leq 1000 \\ 0.00183Re_p\, Re_p \geq 1000 \end{cases} \tag{13}$$

Which

$$Re_p = \frac{\overrightarrow{V}_{nf}d_p\rho_{pf}}{\mu_{nf}} \tag{14}$$

$$\overrightarrow{a} = \overrightarrow{g} - \left(\overrightarrow{V}_{nf}\nabla\right)\overrightarrow{V}_{nf} \tag{15}$$

2.1. Thermophysical properties of nanofluids

To investigate nanofluids flow numerically, it is first necessary to determine their thermophysical properties. According to Das [38] study, nanofluids are different from conventional mixtures and therefore, different models are needed to calculate their thermal properties. In this paper, the density and specific heat equations of the nanofluid can be given as:

$$\rho_{nf} = \alpha_p\rho_p + (1 - \alpha_p)\rho_f \tag{16}$$

$$(\rho c_p)_{nf} = \alpha_p(\rho c_p)_p + (1 - \alpha_p)(\rho c_p)_f \tag{17}$$

Eq. (16) provides a density value. Eq. (17) is the specific heat expression based on the thermal equilibrium assumption of nanoparticles and base fluid [39].

Eq. (19) presents the dynamic viscosity formula for nanofluids proposed by Brinkman [40]. Likewise, Formula 18 predicts the effective thermal conductivity of nanofluids, based on an empirical formula developed by Corcione through a comprehensive analysis of experimental data in the literature [41]. These formulas are crucial to understanding the behavior of nanofluids, and their importance is widely recognized in the scholarly literature.

$$\lambda_{nf} = \lambda_f\left[\frac{(\lambda_p + 2\lambda_f) - 2\alpha_p(\lambda_f - \lambda_p)}{(\lambda_p + 2\lambda_f) + \alpha_p(\lambda_f - \lambda_p)}\right] \tag{18}$$

$$\mu_{nf} = \frac{\mu_f}{(1 - \alpha_p)^{2.5}} \tag{19}$$

2.2. Boundary conditions

The two-dimension rectangular cavity has the following boundary conditions for thermocapillary convection.

$$u = v = 0, T = T_c \quad \text{at } x = 0 \tag{21}$$

$$u = v = 0, \frac{\partial T}{\partial y} = 0 \quad \text{at } y = 0 \tag{22}$$

$$\mu\frac{\partial T}{\partial y} = -Y_T\frac{\partial T}{\partial x}, v = 0, \frac{\partial T}{\partial y} = 0 \text{ at } y = h \tag{23}$$

For the x and y direction velocities, respectively, use u and v.

2.3. Thermophysical parameters of nanofluids

Nanoparticles have a 50 nm diameter and are spherical in shape. The thermophysical properties of nanofluids simulated numerically in this paper are provided in Table 1.

3. Solution method

Discretization of governing equations using the finite element method. For solving discrete equations, the PARDISO solver is utilized, whereas the reverse Euler method is utilized for numerical processing. The evolution of flow field is calculated using the backward difference formulation. The maximum time step is chosen to satisfy the Courant-Friedrichs-Lewy convergence criterion and is determined by the live temperature. Streamlining diffusion and sidewind diffusion is used for the Navier-Stokes and dispersive phase transport equations. Since the oscillatory features of nanofluid thermocapillary convection are being investigated, the average oscillation period is employed as a criterion to evaluate the numerical convergence under consideration in this research. Table 2 displays the average oscillation period of thermocapillary convection at various mesh sizes for mesh A, B, C, and D. Additionally, the mesh processing in this paper refines the mesh at the free surface to better capture the oscillatory processes related to the thermocapillary flow. For the numerical simulation in this research, mesh C is more appropriate when considering the cost of calculation time and numerical precision.

4. Results and discussion

When a small temperature difference is applied to this cavity, a steady thermocapillary convection occurs, resulting in the formation of a stable vortex cell. However, as the temperature difference increases, the thermocapillary convection will transition from a steady-state to an

Table.1
Thermophysical parameters.

Thermal properties	$\rho(kg/m^3)$	$C_p(J/kg\,K)$	$\lambda(W/K\,m)$	$\mu(Pa\cdot s)$	$Y_T(N/K\,m)$
Base fluid (silicon oil) [42]	960	1400	0.11	5.01×10^{-4}	-6.4×10^{-5}
Nanoparticles (Copper) [43]	8970	380	387	/	/

Table 2
Average oscillatory period at different mesh ($\alpha_p = 0.05\ \Delta T = 8$ K).

Mesh	Mesh numbers	Average element quality	Simulation time	Average oscillatory period (s)	Deviation (%)
A	6906	0.8408	3 h 45 min	6.17	6.01
B	12,192	0.8548	6 h 12 min	5.99	3.35
C	18,496	0.8551	7 h 36 min	5.89	1.09
D	23,942	0.8569	9 h 34 min	5.87	——

unsteady-state (oscillation), particularly when the left–right temperature difference surpasses the critical temperature difference. When $\alpha_p = 0.01$, ΔT_{cri} is about 6.45 K. As the temperature difference increases, the flow field gradually becomes unstable, and perturbed vortices start to emerge on the right (cold) side. Once the temperature difference reaches 8 K, the perturbed vortices appear throughout the cavity.

Fig. 2 illustrates the evolution of the flow field throughout one oscillation period at $\Delta T = 8$ K and $\alpha_p = 0.01$. The figure shows that a fixed vortex cell is located near the hot left wall with continuous intensity and position. The convective vortex cells located in the center and right side of the cavity reciprocally migrate from right to left, leading to the separation and merging of vortex cells and generating various flow patterns. For instance, figures (a) to (d) depict the migration of the vortex cell located in the cavity's middle to the right and its merging with the right vortex cell, generating an independent large vortex cell. At the same time, a separate vortex cell is generated near the left vortex cell's free surface corner, gradually increasing in size. Figures (e) to (h) show that the already-formed large vortex cell located on the right side migrates toward the cavity's left side and combines with the middle vortex cell. At the same time, the vortex cell's intensity increases, and a new vortex cell separates at the right wall and free surface corner.

Fig. 3 depicts the temperature contour distribution that corresponds to Fig. 2. Since the left side of the flow field is a fixed vortex, the structure of the isotherm on the left unchanged. The connected portion
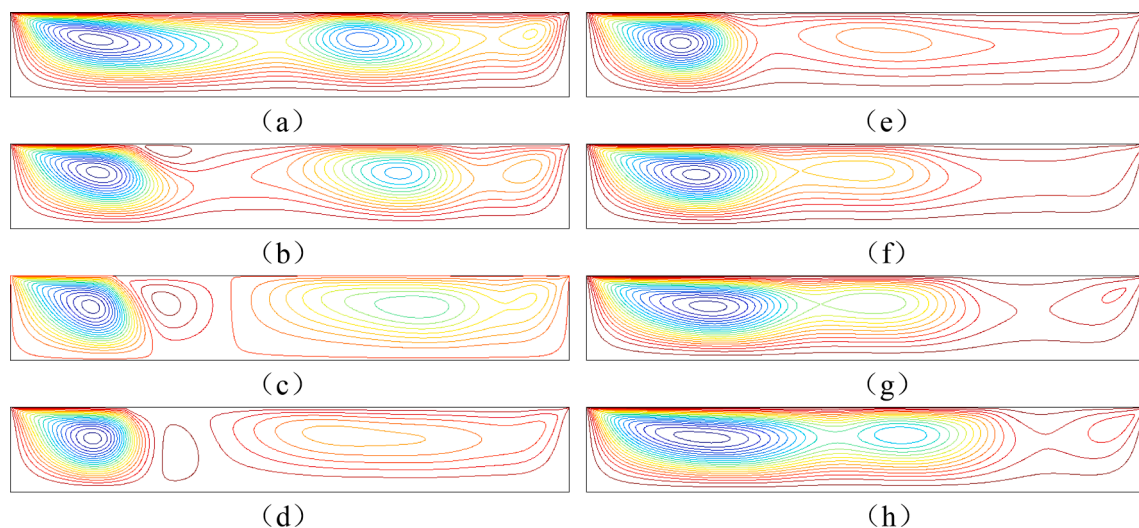

Fig. 2. Vortices evolution as $\Delta T = 8$ K and $\alpha_p = 0.01$ at eight evenly distributed instances within one oscillation period.
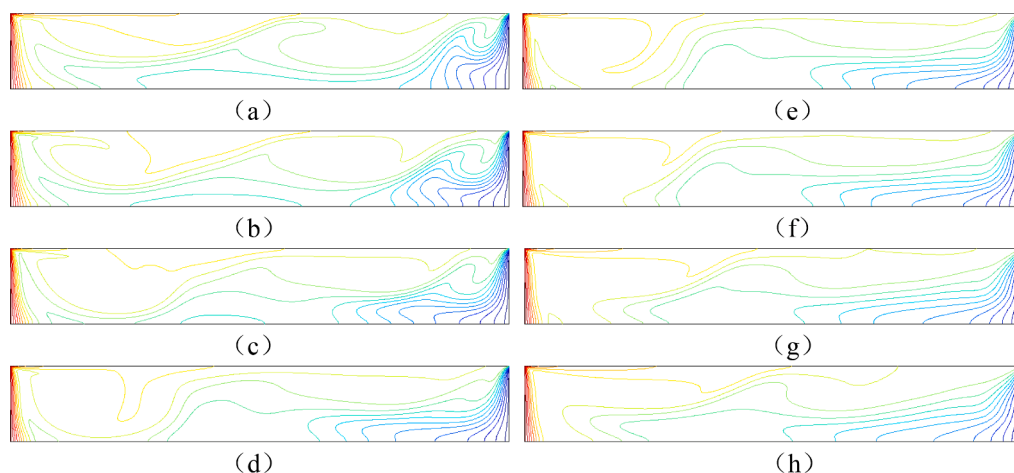

Fig. 3. Isotherms evolution as $\Delta T = 8$ K and $\alpha_p = 0.01$ at eight evenly distributed instances within one oscillation period.

of the vortex cell in the flow field is represented by the central dense isotherm, which periodically migrates to the left. In the thermocapillary convection oscillation, the density of the isotherms coincides with the position of the vortex, suggesting the link between the flow and temperature fields. Meanwhile, a monitoring point was set up at the midpoint of the free surface (x = 10 mm, y = 3 mm) to investigate the instability of nanofluid thermocapillary convection. As can be observed from Fig. 4, the temperature and velocity values at the free surface monitoring point exhibit periodic oscillations.

Since the fluctuations in the rectangular liquid cavity are small. It is difficult to describe the fluctuations clearly by the total velocity or the total temperature. In this paper, the fluctuations of velocity, temperature and flow function are divided into two parts, such as $\psi^{'}(x,y,t) = \psi(x,y,t) - \psi_0(x,y)$, where $\psi(x,y,t)$ is a transient quantity that varies with time, $\psi_0(x,y) = \frac{1}{\tau}\int_0^\tau \varphi(x,y,t)dt$ is a constant time average, $\tau^{'}$ is the length of time well beyond the oscillation period.

Fig. 5 demonstrates the evolution of the fluctuating velocity pattern throughout the entire oscillation period in a two-dimensional rectangular cavity. The study found that the velocity fluctuations can be divided into two regions, upper and lower, based on y = 2/3H. Over the entire oscillation period, two prominent velocity disturbance vortices emerge in the central and right sections of the free surface in the upper region, and three more notable velocity disturbance vortices in the lower region. In the upper area, the velocity fluctuations are more pronounced near the free surface, where they alternate between positive and negative values as they move from the cold end to the hot end. The lower area also shows the same trend, but the range of velocity fluctuations is smaller than that in the upper area. The stratification of the velocity wave throughout the cavity is due to the creation of driving forces on the free surface that make the flow unstable. The velocity fluctuation range in the upper area is larger because the disturbance intensity at this region is larger. Additionally, the velocity changes in the upper and lower regions are opposite in the vertical position. It can also be observed that the maximum fluctuation range is 1.1×10^{-3} during the whole oscillation period, the fluctuation field is very weak compared with the mean field, and the mean-field mainly controls the convection process. As seen in Fig. 6, the fluctuating stream function is composed of several cells that migrate from the cold end to the hot end of the cavity over time, in the same direction as the propagation of the temperature wave, and progressively fill the cavity. The distribution of cell changes periodically during the evolution process, which changes its structure and intensity subsequently. At the same time, the thermocapillary convection oscillatory cell structure in the cavity corresponds to the distribution of the oscillatory fluctuation field.

Fig. 7 shows the relationship between the critical temperature difference and the nanoparticle volume fraction. It is evident from this graph that the critical temperature difference lowers as the nanoparticle volume fraction increases. The above indicates that as the nanoparticle volume fraction increases, overall heat transfer between the fluids intensifies, leading to an instability of the nanofluid thermocapillary convection. This happens because a rise in the nanoparticle volume fraction not only causes the thermal conductivity of the nanofluid to increase, but also causes a decrease in momentum due to the irregular micro-motion, micro-diffusion, and other motions of nanoparticles, which enhance the convective heat transfer, resulting in the nanoparticle thermocapillary convection becoming less stable.

Because the two-phase mixture model varies from the single-phase model in that it considers the slip velocity between nanoparticles and the base liquid, the critical temperature differences determined using the two models are different for the same volume fraction. To better represent the difference between the two models for the critical temperature difference, the essential concept of temperature difference ratio is used, i.e., the critical temperature difference calculated with the two-phase mixture model divided by the critical temperature difference calculated with the single-phase model. The blue line in Fig. 7 indicates the critical temperature difference ratio versus volume fraction. When the nanoparticle volume fractions are low, the critical temperature difference ratio is relatively small, indicating that the difference between the single-phase model and the two-phase mixture model is significant under these conditions. As the volume fraction increases, the critical temperature difference rate remains stable at about 0.92, showing little distinction between the two models' results. This is primarily due to the fact that the single-phase equation is valid at appropriate thermophysical properties. However, when a little volume fraction is added to a fluid, the fluid's thermophysical properties are drastically altered in comparison to their original state. Therefore, the difference in calculation with a single-phase model is large. In addition, the difference between the two models diminishes as the volume fraction increases.

Fig. 8 shows the distribution of the fluctuating temperature field at different nanoparticle volume fractions for $\Delta T = 8$ K. Since the temperature fluctuation varies throughout the oscillation, we provide the temperature fluctuation distribution when the temperature at the monitoring point reaches its lowest point during the oscillation. The illustration demonstrates that while the strength of the temperature wave fluctuates for various volume fractions, the distribution's basic shape remains the same, showing the nanoparticle volume fraction affects the thermocapillary convective instability, but the effect is weak.
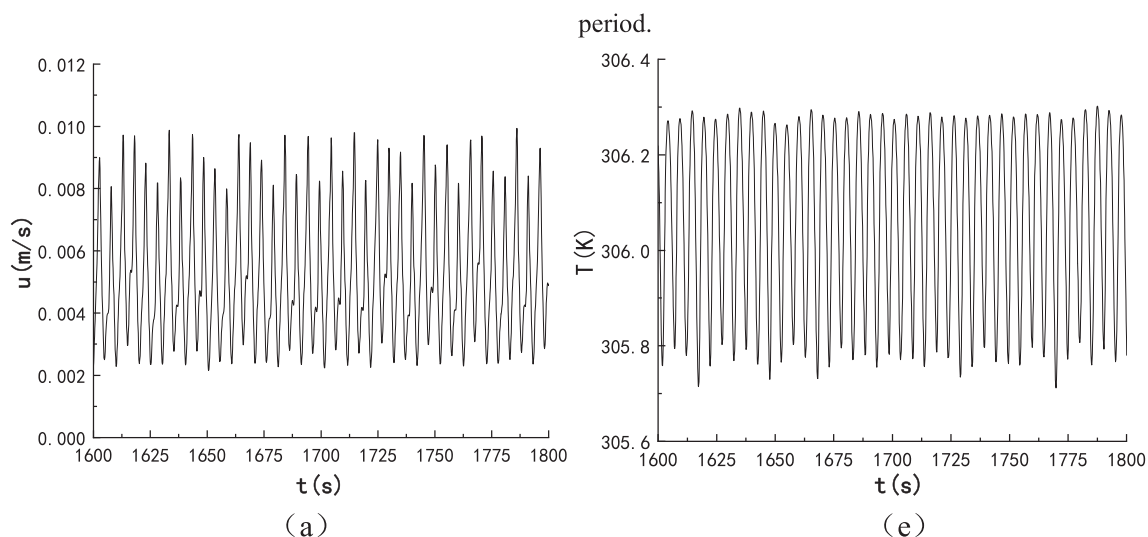
period.

Fig. 4. Velocity (a) and temperature (b) time histories at monitoring points at the free surface (L/2, H) as $\Delta T = 8$ K and$\alpha_p = 0.02$.
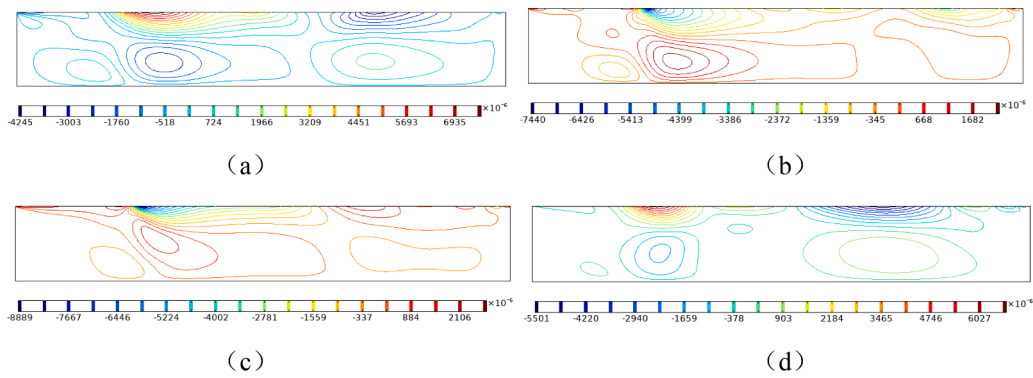
Fig. 5. Velocity disturbances evolution as $\Delta T = 8$ K and $\alpha_p = 0.01$ at four evenly distributed instances within one oscillation period.
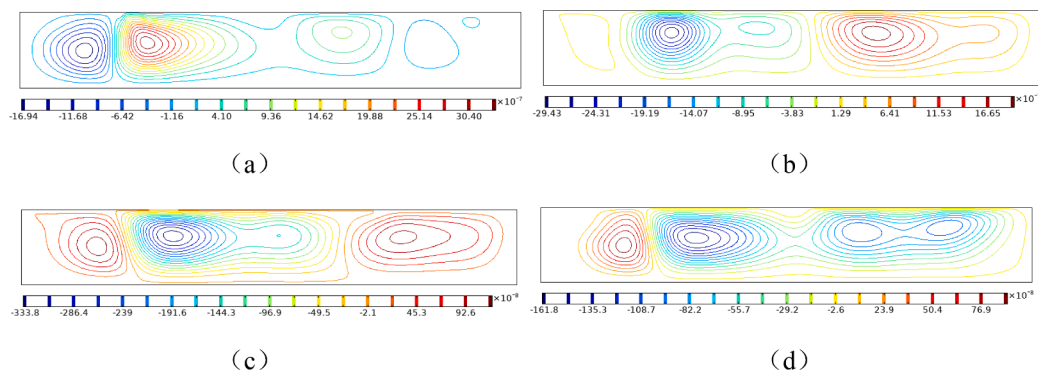

Fig. 6. Stream function disturbances as $\Delta T = 8$ K and $\alpha_p = 0.01$ at four evenly distributed instances within one oscillation period.
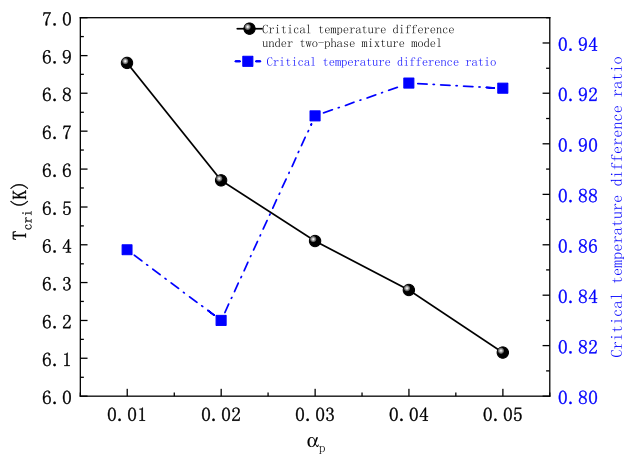

Fig. 7. Variation of the critical temperature difference with nanoparticle volume fraction using two-phase mixture model (black); Variation of the critical temperature difference ratio with nanoparticle volume fraction (blue).

From Fig. 8, it is clear that increasing the nanoparticle volume fractions can enhance heat transfer overall and reduce the critical temperature difference, but increasing the nanoparticle volume fractions at a particular time during oscillation does not necessarily enhance heat transfer, as shown in Fig. 8. Fig. 8 reveals that the range of temperature changes grows as the volume fraction rises, indicating that the heat transmission effect diminishes gradually as the nanoparticle volume fraction rises. This is because, while both the nanofluid's viscosity and thermal conductivity increase proportionally with volume fraction, the negative effect of the former is much more pronounced than the latter.

Also, there is a significant separation between the centers of the positive and negative disturbance waves. This suggests that the disturbance wave becomes extremely unstable at a temperature difference of $\Delta T = 8$ K.

Fig. 9 gives the fluctuation velocity field for different nanoparticle volume fractions at $\Delta T = 8$ K. Since the velocity fluctuations are varied during one oscillation period, the distribution of the velocity fluctuations at the peak of the temperature value at the monitoring point is given. The velocity fluctuation distribution does not change with volume fraction. Additionally, the range of velocity variation tends to diminish as a result of the nanoparticles increasing the fluid's viscosity. Fig. 10 shows that the cells in the left area of the fluctuating flow function field are negative, and the cells in the other areas are positive, which indicates a fluctuation pattern different from the nanofluid thermocapillary convection and similar to temperature fluctuation. Notably, as the volume fraction of nanoparticles declines, the fluctuation range of the flow function also gradually shrinks, and the flow function's fluctuation exhibits a time-evolving trend. In addition, changing the nanoparticle volume fraction doesn't change the general structure of the flow function fluctuation cell element in the whole cavity, but the flow function fluctuation is slightly enhanced near the left wall, and new vortex cells emerge.

The velocity oscillation time histories of the monitoring points at different nanoparticle volume fractions at $\Delta T = 8$ K are presented in Fig. 11. As observed, the velocity evolution process demonstrates comparable oscillation characteristics at different nanoparticle volume fractions, but there are variations in the oscillation range and oscillation period of the velocity. Notably, an increase in volume fraction leads to a significant reduction in the maximum and minimum velocities, making them more uniform. Fig. 12 illustrates that an increase in volume fraction results in a decreased amplitude and an elongated velocity oscillation period. This observation implies that nanoparticle volume
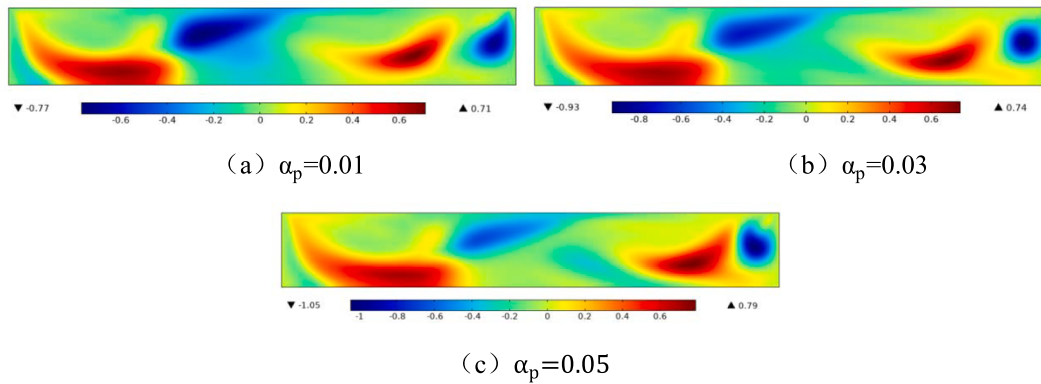
（a）α_p=0.01 　　（b）α_p=0.03

（c）α_p=0.05

Fig. 8. Temperature fluctuation distribution under different nanoparticles volume fractions as$\Delta T = 8$ K.

（a）α_p=0.01 　　（b）α_p=0.03

（c）α_p=0.05
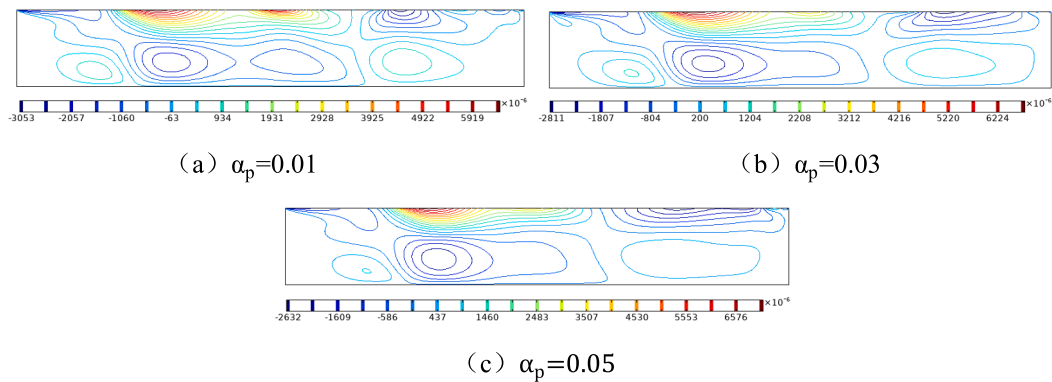
Fig. 9. Velocity fluctuation distribution under different nanoparticles volume fractions as$\Delta T = 8$ K.

（a）α_p=0.01 　　（b）α_p=0.03

（c）α_p=0.05
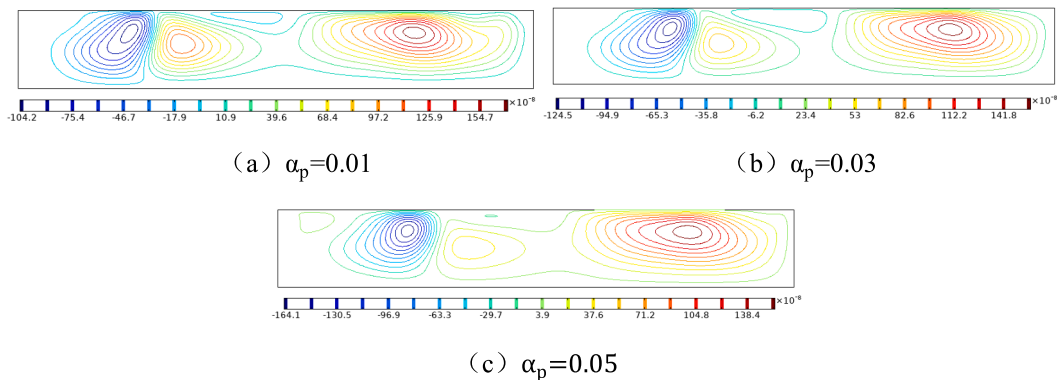
Fig. 10. Stream function fluctuation distribution under different nanoparticles volume fractions as$\Delta T = 8$ K.

fraction may govern the oscillation characteristics of thermocapillary convection.

Thermocapillary convection is generated by a temperature gradient on the free surface of a rectangular liquid cavity. The velocity of the free surface is a critical parameter that affects the fluid flow throughout the entire cavity. Because the velocity at the monitoring point is oscillating, the surface velocity distribution at different volume fractions for the velocity values of the monitoring point at the peak is given. As shown in Fig. 13, the velocity is dramatically higher near the hot and cold walls because of the substantial temperature gradient in that area. Meanwhile, the free surface velocity near the hot end decreases as the nanoparticle volume fraction increases, which is due to the increase of the nanoparticle volume fraction, which increases the viscosity of the fluid and

the resistance of fluid motion during the flow, so the nanoparticle volume fraction is a significant factor affecting the resistance to nanofluid flow. There is also a general tendency in the free surface velocity, and it is affected by the volume fraction.

Fig. 14 displays the horizontal velocity curve for various nanoparticle volume fractions at $\times$ = L/2., where the flow velocity decreases continuously with increasing volume fraction, but the shape is generally similar. This trend is related to a rise in dynamic viscosity brought on by the growth of volume fractions, resulting in smaller velocities. For a specific volume fraction of nanoparticle, the horizontal velocity undergoes an increasing–decreasing-increasing process as y increases, and the velocity at the free surface is approximately three times the return velocity at y = 1/3H. This is because the thermocapillary convection is
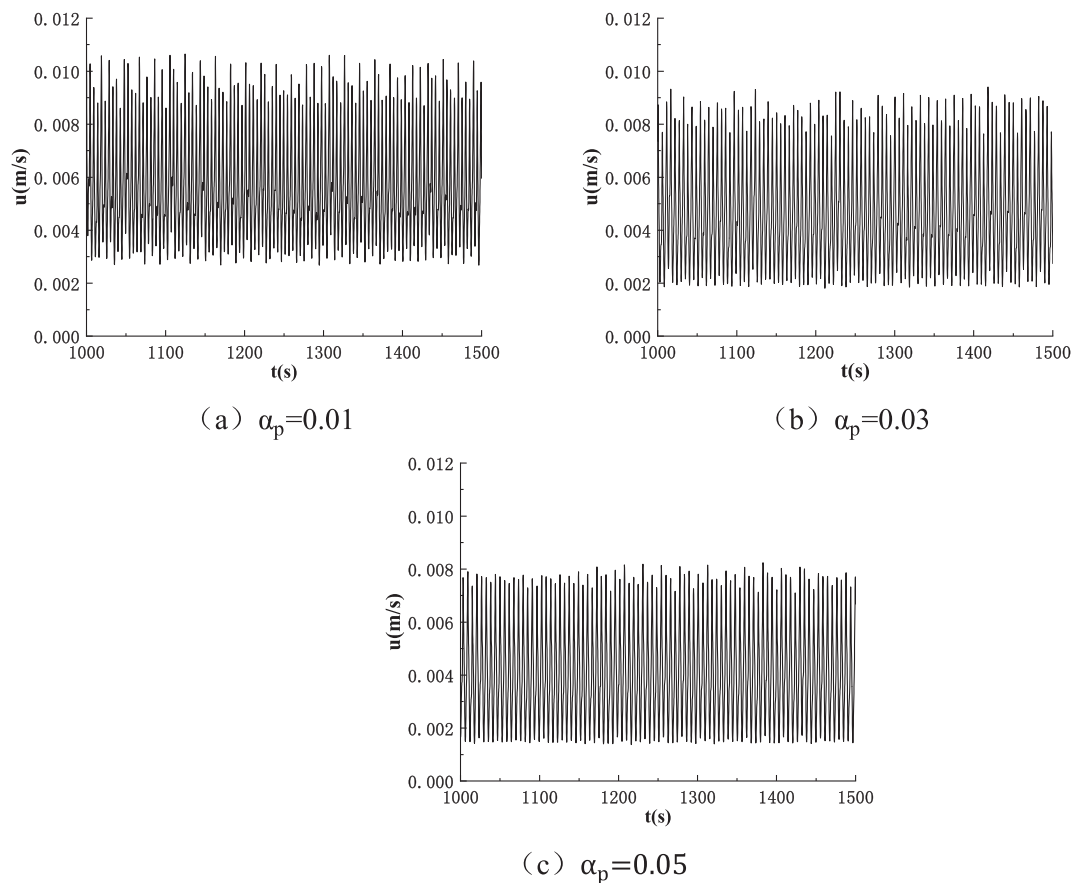
（a）α_p=0.01

（b）α_p=0.03

（c）α_p=0.05

Fig. 11. Time histories of velocity fluctuations at the free surface monitoring point at ΔT = 8 K with different volume fractions.
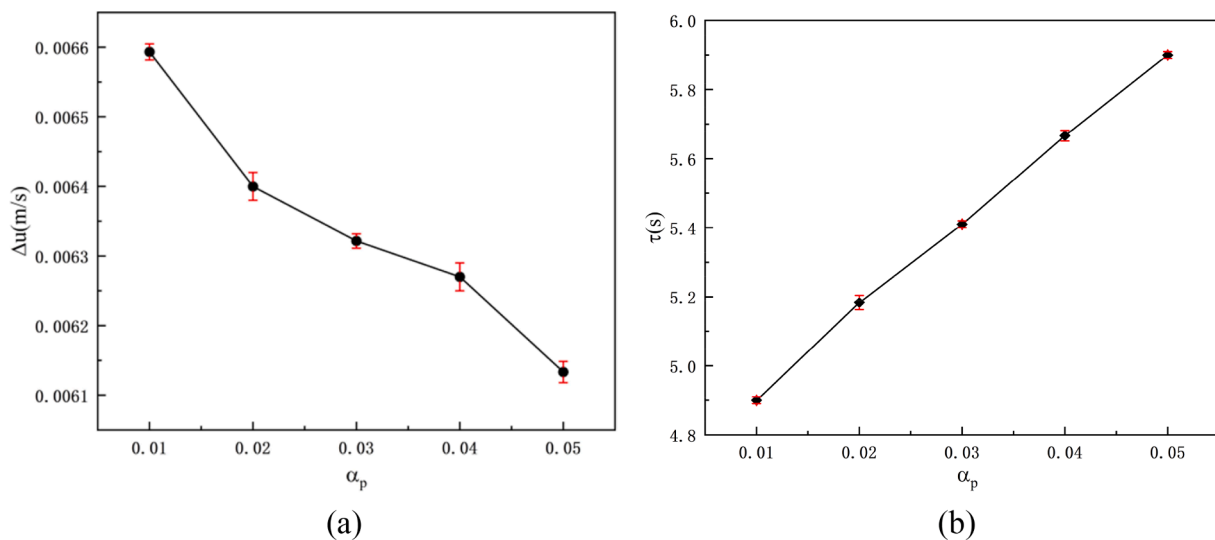

(a)

(b)

Fig. 12. Variation of average velocity oscillatory amplitude (a) and period (b) at monitoring point with nanoparticle volume fraction asΔT = 8 K.

driven by the free surface, which is greater than the velocity inside the cavity. At this moment, there is a steady reflux in the rectangular cavity.

From Fig. 15, It is demonstrated that the volume fraction reduces and increases dramatically near the hot and cold walls of the horizontal median, whereas the volume fraction is uniformly distributed in the remaining portions of the horizontal median. Notably, the volume fraction fluctuates more obviously on the bottom boundary, where it decreases and increases sharply at the hot and cold walls, respectively. In addition, the volume fraction generally shows a decreasing trend from

the cold end to the hot end. The mentioned phenomenon is brought on by thermocapillary force formed by the effect of the temperature gradient driving the flow of fluid from the hot end to the cold end; the fluid sinks at the cold end, increasing the volume fraction of particles at the cold end's bottom, and the volume fraction from the cold end to the hot end decreases due to the fluid viscosity inside the formation of reflux. Repeated reflux leads to a decreasing particles volume fraction at the hot end and an increasing particles volume fraction at the cold end. The above similar phenomena are observed for other volume fractions of
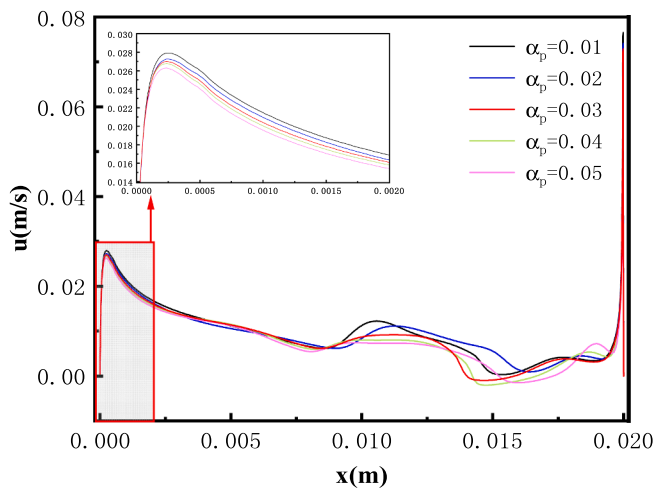
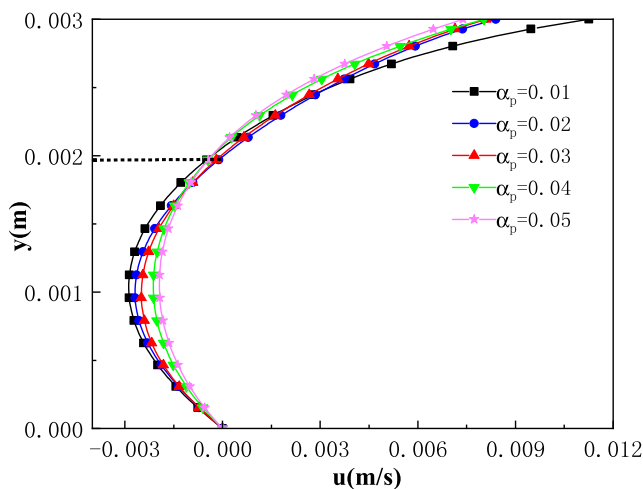**Fig. 13.** Free surface velocity for different nanoparticle volume fractions.

Fig. 14. Distribution of velocities at various nanoparticle volume fractions at x = L/2.
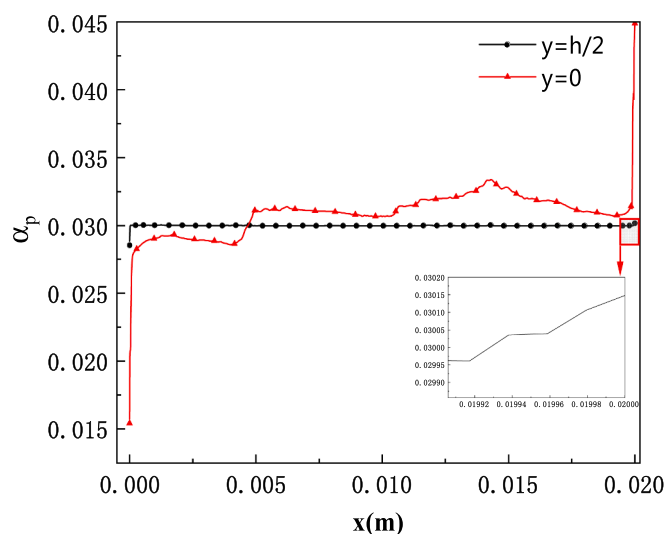

Fig. 15. Volume fraction distribution of nanoparticles on the horizontal midline and bottom boundary at $\Delta T = 8K$ and $\alpha_p = 0.03$.

nanofluids, suggesting that the non-homogeneity of the nanoparticle volume fraction during thermocapillary oscillation is mainly near the walls.

5. Conclusion

In previous studies, the nanofluid thermocapillary convection instability within a rectangular cavity was investigated using a single-phase model. However, given the higher accuracy of the two-phase mixture model compared to the single-phase model, this study adopts the two-phase mixture model to analyze the oscillatory characteristics of thermocapillary convection in nanofluids. Additionally, the study compares the disparity in critical temperature differences between the single-phase model and the two-phase mixture model. Following are the specific conclusions:

1) With increasing nanoparticle volume fraction from 0.01 to 0.05, the critical temperature difference decreases from 6.88 K to 6.1 K and the velocity oscillation amplitude from 0.0066 m/s to 0.0061 m/s, whereas the period of the oscillation grows linearly from 4.9 K to 5.9 K.
2) The fluctuation ranges of temperature wave and flow functions in the whole flow field rise with increasing nanoparticle volume fraction, but ranges of velocity variations decrease.
3) The non-homogeneity of the nanoparticle volume fraction is most pronounced in the vicinity of the walls in the thermocapillary convection oscillation process.
4) The critical temperature differences obtained using the two-phase mixture model are less than that obtained by the single-phase model. Additionally, the difference between the two models for the critical temperature difference get less as nanoparticles volume fraction rises.

CRediT authorship contribution statement

Xiaoming Zhou: Conceptualization, Methodology, Software. **Cheng Dai:** Data curation. **Yanni Jiang:** Supervision. **Qisheng Chen:** Writing – review & editing.

Declaration of Competing Interest

The authors declare that they have no known competing financial interests or personal relationships that could have appeared to influence the work reported in this paper.

Data availability

Data will be made available on request.

Acknowledgments

References

[1] X. Zhou, X. Huai, Thermosolutocapillary Convection in an Open Rectangular Cavity With Dynamic Free Surface, J. Heat Transf. 137 (2015), 082901.
[2] J.J. Yu, D.F. Ruan, Y.R. Li, J.C. Chen, Experimental study on thermocapillary convection of binary mixture in a shallow annular pool with radial temperature gradient, Experimental Thermal and Fluid Science 61 (2015) 79–86.
[3] Y.W. Jia, W.Y. Shi, T.S. Wang, Experimental Investigation on Marangoni Convection Instability Induced by Evaporation in a Sessile Droplet of Silicone Oil on a Heated Substrate, K, Cheng Je Wu Li Hsueh PaoJournal Eng. Thermophys. 38 (2017) 2001–2004.

[4] S. Yang, R. Liang, S. Xiao, J. He, S. Zhang, Influence of Ambient Airflow on Free Surface Deformation and Flow Pattern Inside Liquid Bridge With Large Prandtl Number Fluid (Pr > 100) Under Gravity, J. Heat Transf. 139 (2017).

[5] X. Zhou, X. Huai, Free Surface Deformation of Thermo-Solutocapillary Convection in Axisymmetric Liquid Bridge, Microgravity Science and Technology 27 (1) (2015) 39–47.

[6] Y. Yang, L. Pan, J. Xu, Effects of microgravity on Marangoni convection and growth characteristic of a single bubble, Acta Astronautica 100 (2014) 129–139.

[7] H. Huang, G. Zhu, Y. Zhang, Effect of Marangoni number on thermocapillary convection in a liquid bridge under microgravity, International Journal of Thermal Sciences 118 (2017) 226–235.

[8] S.U.S. Choi, J. Eastman, Enhancing thermal conductivity of fluids with nanoparticles, in: 1995.

[9] H. Bazdar, D. Toghraie, F. Pourfattah, O.A. Akbari, H.M. Nguyen, A. Asadi, Numerical investigation of turbulent flow and heat transfer of nanofluid inside a wavy microchannel with different wavelengths, Journal of Thermal Analysis and Calorimetry 139 (3) (2020) 2365–2380.

[10] H. Arasteh, R. Mashayekhi, M. Goodarzi, S.H. Motaharpour, M. Dahari, D. Toghraie, Heat and fluid flow analysis of metal foam embedded in a double-layered sinusoidal heat sink under local thermal non-equilibrium condition using nanofluid, Journal of Thermal Analysis and Calorimetry 138 (2) (2019) 1461–1476.

[11] W. He, B. Ruhani, D. Toghraie, N. Izadpanahi, N.N. Esfahani, A. Karimipour, M. Afrand, Using of Artificial Neural Networks (ANNs) to predict the thermal conductivity of Zinc Oxide-Silver (50%–50%)/Water hybrid Newtonian nanofluid, Int. Commun. Heat Mass Transf. 116 (2020), 104645.

[12] A. Boroomandpour, D. Toghraie, M. Hashemian, A comprehensive experimental investigation of thermal conductivity of a ternary hybrid nanofluid containing MWCNTs- titania-zinc oxide/water-ethylene glycol (80:20) as well as binary and mono nanofluids, Synthetic Metals 268 (2020), 116501.

[13] C.B. Shi, Y.N. Jiang, G. Yin, et al., Three-dimensional numerical simulation of dynamic characteristics of flue gas reheater, Electric power technology and environmental protection 38 (3) (2022) 215–223.

[14] M. Sheikholeslami, New computational approach for exergy and entropy analysis of nanofluid under the impact of Lorentz force through a porous media, Computer Methods in Applied Mechanics and Engineering 344 (2019) 319–333.

[15] M. Sheikholeslami, Numerical approach for MHD Al2O3-water nanofluid transportation inside a permeable medium using innovative computer method, Computer Methods in Applied Mechanics and Engineering 344 (2019) 306–318.

[16] M. Sheikholeslami, Influence of magnetic field on Al2O3-H2O nanofluid forced convection heat transfer in a porous lid driven cavity with hot sphere obstacle by means of LBM, Journal of Molecular Liquids 263 (2018) 472–488.

[17] M. Sheikholeslami, S.A. Shehzad, Z. Li, A. Shafee, Zhixiong Li, Ahmad Shafee, Numerical modeling for alumina nanofluid magnetohydrodynamic convective heat transfer in a permeable medium using Darcy law, International Journal of Heat and Mass Transfer 127 (2018) 614–622.

[18] M. Sheikholeslami, A. Zeeshan, Analysis of flow and heat transfer in water based nanofluid due to magnetic field in a porous enclosure with constant heat flux using CVFEM, Computer Methods in Applied Mechanics and Engineering 320 (2017) 68–81.

[19] Z. Khalili, M. Sheikholeslami, Numerical modeling for efficiency of solar cell module combined with TEG involving Fe3O4-water nanofluid utilizing MHD, Journal of Magnetism and Magnetic Materials 580 (15) (2023), 170950.

[20] M. Sheikholeslami, Efficacy of porous foam on discharging of phase change material with inclusion of hybrid nanomaterial, The Journal of Energy Storage 62 (3) (2023), 106925.

[21] M. Sheikholeslami, H.R.A. Al-Hussein, Modification of heat storage system involving Trombe wall in existence of paraffin enhanced with nanoparticles, The Journal of Energy Storage 58 (9) (2023), 106419.

[22] N.K. Gupta, A.K. Tiwari, S.K. Ghosh, Heat transfer mechanisms in heat pipes using nanofluids-A review, Experimental Thermal and Fluid Science 90 (2018) 84–100.

[23] W. Du, J. Zhao, H. Li, Y. Zhang, J. Wei, K. Li, Thermal Dynamics of Growing Bubble and Heat Transfer in Microgravity Pool Boiling, in: W. Hu, Q. Kang (Eds.), Phys. Sci. Microgravity Exp. Board SJ-10 Recover, Satell., Springer, Singapore, 2019, pp. 73–99.

[24] A.Z. Stetten, S.V. Iasella, T.E. Corcoran, S. Garoff, T.M. Przybycien, R.D. Tilton, Surfactant-induced Marangoni transport of lipids and therapeutics within the lung, Current Opinion in Colloid & Interface Science 36 (2018) 58–69.

[25] H. Aminfar, M. Mohammadpourfard, F. Mohseni, Numerical investigation of thermocapillary and buoyancy driven convection of nanofluids in a floating zone, International Journal of Mechanical Sciences 65 (1) (2012) 147–156.

[26] H. Saleh, I. Hashim, Buoyant Marangoni convection of nanofluids in square cavity, Applied Mathematics and Mechanics 36 (9) (2015) 1169–1184.

[27] L. Kolsi, H.F. Oztop, A. Alghamdi, N. Abu-Hamdeh, M.N. Borjini, H.B. Aissia, A computational work on a three dimensional analysis of natural convection and entropy generation in nanofluid filled enclosures with triangular solid insert at the corners, Journal of Molecular Liquids 218 (2016) 260–274.

[28] M. Sheikholeslami, A.J. Chamkha, Influence of Lorentz forces on nanofluid forced convection considering Marangoni convection, Journal of Molecular Liquids 225 (2017) 750–757.

[29] A.A. Abdullah, S.A. Althobaiti, K.A. Lindsay, Marangoni convection in water-alumina nanofluids: Dependence on the nanoparticle size, Eur. J. Mech. - BFluids. 67 (2018) 259–268.

[30] G.S. Gevorgyan, K.A. Petrosyan, R.S. Hakobyan, R.B. Alaverdyan, Experimental investigation of Marangoni convection in nanofluids, J. Contemp. Phys. Armen. Acad. Sci. 52 (4) (2017) 362–365.

[31] Y. Jiang, X. Zhou, Analysis of flow and heat transfer characteristics of nanofluids surface tension driven convection in a rectangular cavity, International Journal of Mechanical Sciences 153-154 (2019) 154–163.

[32] X. Zhou, F. Chi, Y. Jiang, Q. Chen, Moderate Prandtl Number Nanofluid Thermocapillary Convection Instability in Rectangular Cavity, Microgravity Science and Technology 34 (2022) 24.

[33] Y. Jiang, Z. Xu, Numerical Investigation of Nanofluid Thermocapillary Convection Based on Two-Phase Mixture Model, Microgravity Science and Technology 29 (5) (2017) 365–370.

[34] C. Chen, S. Feng, H. Peng, X. Peng, L. Chaoyue, R. Zhang, Thermocapillary convection flow and heat transfer characteristics of graphene nanoplatelet based nanofluid under microgravity, Microgravity Science and Technology 33 (2021) 40.

[35] M. Mikko, T. Veikko, K. Sirpa, On the mixture model for multiphase flow, VTT Publ. 288 (1996).

[36] M. Manninen, V. Taivassalo, S. Kallio, Mixture Model for Multiphase Flow, (1996).

[37] L. Schiller, A drag coefficient correlation, VDI Ztg. 77 (1935).

[38] Science and Technology, Nanofluids, 2008.

[39] K. Khanafer, K. Vafai, A critical synthesis of thermophysical characteristics of nanofluids, International Journal of Heat and Mass Transfer 54 (19-20) (2011) 4410–4428.

[40] H.C. Brinkman Bosscha Physics Laboratory, University of Indonesia, Bandung, Indonesia The viscosity of concentrated suspensions and solutions J. Chem. Phys. 20 4 1952 1952 571 571.

[41] M. Corcione, Empirical correlating equations for predicting the effective thermal conductivity and dynamic viscosity of nanofluids, Energy Convers. Manag. 52 (1) (2011) 789–793.

[42] M. Teitel, D. Schwabe, A.Y. Gelfgat, Experimental and computational study of flow instabilities in a model of Czochralski growth, Journal of Crystal Growth 310 (7-9) (2008) 1343–1348.

[43] X. Zhou, F. Chi, Y. Jiang, Q. Chen, Numerical investigation of thermocapillary convection instability for large Prandtl number nanofluid in rectangular cavity, Int. Commun. Heat Mass Transf. 133 (2022), 105956.